JHEP

Published for SISSA by Springer

Received: August 12, 2025
Revised: October 8, 2025
Accepted: October 28, 2025
Published: December 19, 2025

# Sensitivity of an early dark matter search using the electromagnetic calorimeter as a target for the Light Dark Matter eXperiment

**The LDMX collaboration**

**Torsten Åkesson**,[a] **Elizabeth Berzin**,[b] **Cameron Bravo**,[c] **Liam Brennan**,[d] **Lene Kristian Bryngemark**,[a] **Pierfrancesco Butti**,[c] **Filippo Delzanno**,[d] **E. Craig Dukes**,[e] **Valentina Dutta**,[f] **Bertrand Echenard**,[g] **Ralf Ehrlich**,[e] **Thomas Eichlersmith**,[h,*] **Einar Elén**,[a] **Andrew Furmanski**,[h] **Victor Gomez**,[g] **Matt Graham**,[c] **Chiara Grieco**,[d] **Craig Group**,[e] **Hannah Herde**,[a] **Christian Herwig**,[i] **David G. Hitlin**,[g] **Tyler Horoho**,[e] **Joseph Incandela**,[d] **Nathan Jay**,[g] **Asahi Jige**,[d] **Wesley Ketchum**,[j] **Gordan Krnjaic**,[j] **Amina Li**,[d] **Zihan Ma**,[d] **Jeremiah Mans**,[h] **Cristina Mantilla Suarez**,[e] **Sanjit Masanam**,[d] **Phillip Masterson**,[d] **Steven Metallo**,[h] **Sophie Middleton**,[g] **Joseph Muse**,[h] **Timothy Nelson**,[c] **Rory O'Dwyer**,[b] **James Oyang**,[g] **Jessica Pascadlo**,[e] **Emrys Peets**,[c] **Luis Sarmiento Pico**,[a] **Ruth Pöttgen**,[a] **Philip Schuster**,[c] **Chris Sellgren**,[d] **Lauren Tompkins**,[b] **Natalia Toro**,[c] **Nhan Tran**,[j] **Tamas Vami**,[d] **Erik Wallin**,[a] **Yuxuan Wang**,[d] **Andrew Whitbeck**,[j] **Duncan Wilmot**,[d] **Xinyi Xu**[d] **and Danyi Zhang**[d]

[a] *Lund University, Department of Physics, Box 118, 221 00 Lund, Sweden*
[b] *Stanford University, Menlo Park, CA 94025, U.S.A.*
[c] *SLAC National Accelerator Laboratory, Menlo Park, CA 94025, U.S.A.*
[d] *University of California at Santa Barbara, Santa Barbara, CA 93106, U.S.A.*
[e] *University of Virginia, Charlottesville, VA 22904, U.S.A.*
[f] *Carnegie Mellon University, Pittsburgh, PA 15213, U.S.A.*
[g] *California Institute of Technology, Pasadena, CA 91125, U.S.A.*
[h] *University of Minnesota, Minneapolis, MN 55455, U.S.A.*
[i] *University of Michigan, Ann Arbor, MI 48109, U.S.A.*
[j] *Fermi National Accelerator Laboratory, Batavia, IL 60510, U.S.A.*

[*] Corresponding author.



https://doi.org/10.1007/JHEP12(2025)150

*E-mail:* ldmx-pubs@slac.stanford.edu, eichl008@umn.edu

Abstract: The Light Dark Matter eXperiment (LDMX) is proposed to employ a thin tungsten target and a multi-GeV electron beam to carry out a missing momentum search for the production of dark matter candidate particles. We study the sensitivity for a complementary missing-energy-based search using the LDMX Electromagnetic Calorimeter as an active target with a focus on early running. In this context, we construct an event selection from a limited set of variables that projects sensitivity into previously-unexplored regions of light dark matter phase space — down to an effective dark photon interaction strength $y$ of approximately $2 \times 10^{-13}$ ($5 \times 10^{-12}$) for a 1 MeV (10 MeV) dark matter candidate mass.

Keywords: Dark Matter, Fixed Target Experiments

ArXiv ePrint: 2508.08121

JHEP12(2025)150

## Contents



## 1 Introduction

The origin and nature of dark matter (DM) remains among the most elusive areas of modern physics [1–5]. The a priori extremely large viable mass range of DM candidates can be significantly narrowed by assuming thermal contact of DM with ordinary matter in the early universe [6, 7]. The MeV to GeV mass region of thermal DM remains relatively unexplored, corresponds to the range where other matter is stable over the lifetime of the universe, and can be probed in accelerator-based fixed target experiments [8, 9].

The planned Light Dark Matter eXperiment (LDMX) [10, 11] is designed to observe the production of sub-GeV thermal DM and is anticipated to be constructed by the end of the decade. In the nominal scenario, electrons incident on a thin target undergo a dark bremsstrahlung (DB) process (inset in figure 1) where non-interacting DM particles are radiated through a dark mediator. The detector design allows for measuring the missing momentum carried by the DM particles through the measurement of the recoil electron track. It includes a spectrometer dipole; a silicon tracker with sections before and after the thin target; a high-granularity Si-Tungsten Electromagnetic Calorimeter (ECal) with a depth of forty radiation lengths; and a Hadronic Calorimeter (HCal) as well as a scintillator-bar detector for electron counting. LDMX will take data with a high-rate, low-intensity electron beam with a typical current of one electron every 27 ns extracted from the Linac Coherent Light Source II (LCLS-II) at SLAC [12]. The primary beam energy is expected to be 8 GeV using a planned upgrade to LCLS-II, however some data may be acquired with 4 GeV depending on the accelerator and detector schedules.

The use of a thin target requires $4\times10^{14}$ electrons-on-target (EoT) to obtain the sensitivity projected for the first phase of LDMX [13]. However, the majority of beam electrons pass through the target without significant interactions and then enter the ECal at full energy. Given the density of material composing the ECal and the fine-grained ECal readout, the

ECal can be considered as a second effective target mass for LDMX. In this approach, the components of the recoil electron momentum cannot be individually measured, which results in a measurement of missing energy instead of missing momentum. Given the thickness of the ECal, the effective luminosity of such a measurement can be higher than that with the thin target, though the available handles for managing background are fewer. This paper quantifies the sensitivity of a search using the LDMX ECal as a target for a first result with $10^{13}$ EoT, equivalent to about two weeks of nominal LDMX beam exposure. Scenarios where this initial exposure results from both a 4 GeV or 8 GeV beam are discussed in this paper.

The paper is organized as follows: in section 2 the LDMX detector design used in this study is reviewed, as well as the signal and background characteristics. The samples of simulated events are summarized in section 3. In section 4, the analysis strategy is described. The results and conclusions are discussed in section 5 and 6.

## 2 The LDMX detector

LDMX will utilize a high-rate, low-current electron beam incident on a thin, solid (tungsten) target to search for light thermal DM. The behavior of DM production is benchmarked by a dark bremsstrahlung process, where electrons emit a dark mediator or dark photon ($A'$) suppressed by the mixing strength $\epsilon \ll 1$. In turn, the $A'$ subsequently decays to non-interacting DM particles ($\chi$) which escape the detector leaving an energy imbalance relative to the initial beam energy.

The LDMX detector, as diagrammed in figure 1, is designed to reject the high rate of background events, including rare photon-nuclear (PN) and electron-nuclear (EN) reactions. The tracking system consists of a tagging tracker utilizing a 1.5 T magnetic field to measure the electron's incident momentum and a recoil tracker utilizing the magnet's fringe field to measure the momentum of charged particles leaving the target. The ECal measures the recoil electron energy as well as interactions that may result from other forward particles that are produced in background processes. In addition, a sampling HCal composed of steel absorber layers and scintillator bars read out by silicon photo-multipliers provides additional background rejection capabilities particularly for events with energetic neutral hadrons.

The ECal design for LDMX is adopted from the CMS High Granularity Calorimeter for the CMS Phase-2 upgrade [14] which fulfills requirements for a fast, efficient, and finely-segmented electromagnetic calorimeter system. The ECal, diagrammed in figure 2, is a sampling calorimeter with 34 layers organized into 17 double-sided planes, corresponding to approximately 40 $X_0$ of material. This large material budget contributes to both an increased rate of DB production relative to the 0.1 $X_0$ thin target, as well as excellent electromagnetic shower containment. Each ECal layer contains tungsten absorbers as well as printed circuit boards (PCB) for services and data transport to and from silicon sensors. The sensors each contain 432 readout pads and there are seven sensors arranged in a "flower" (figure 2), providing precise transverse shower reconstruction capable of distinguishing individual electromagnetic showers with small angular separation. The first pre-shower layer is not preceded by tungsten absorber in order to prevent the shower from beginning before a sensitive layer.

The primary physics trigger of LDMX is based on the observation of missing energy in the ECal. For a single incoming electron, the trigger requires the total reconstructed



JHEP12(2025)150

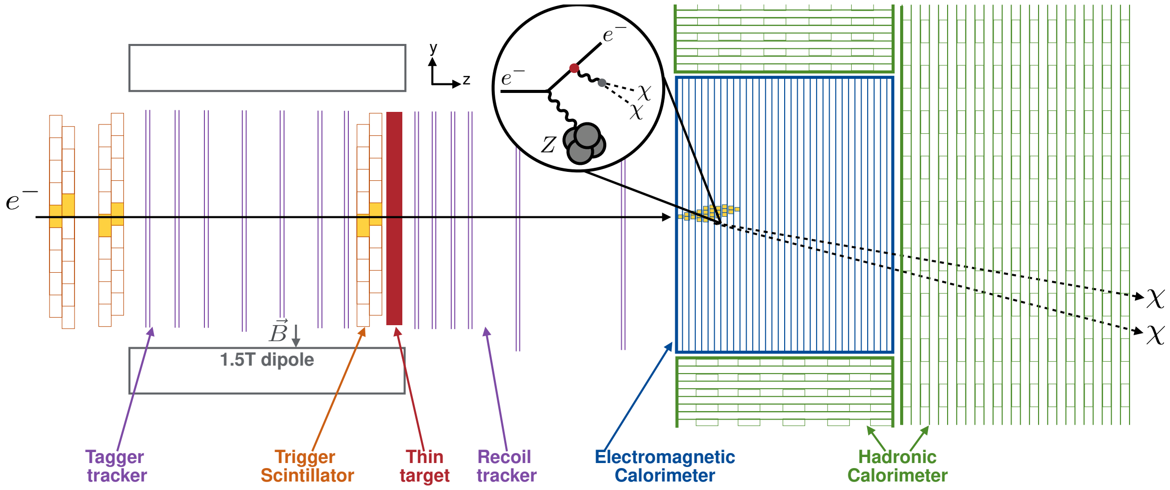


**Figure 1.** A diagram of the LDMX detector apparatus, illustrating production of DM in the ECal from a scattering electron, and the corresponding response of the various sub-systems.

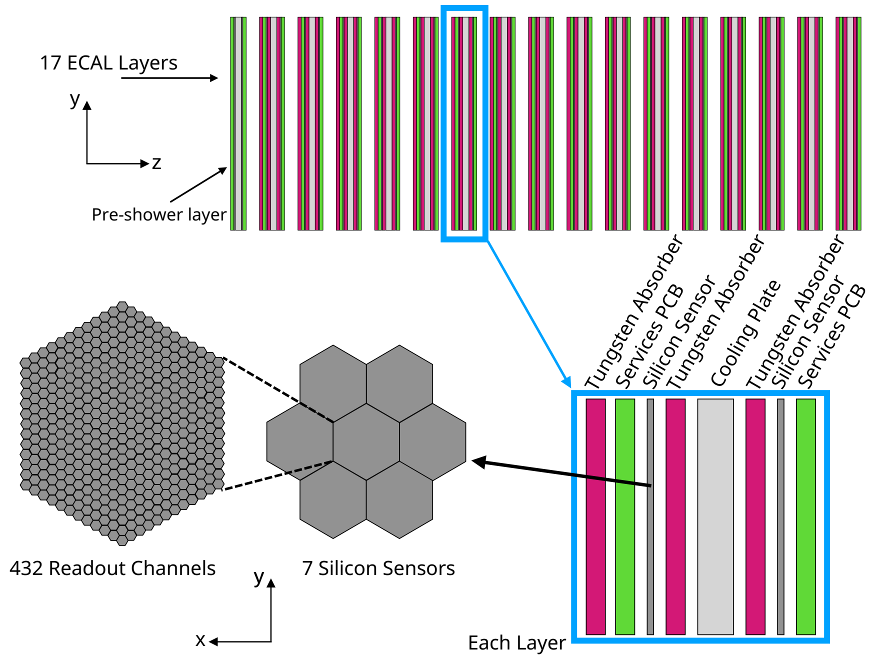


**Figure 2.** A diagram of the LDMX ECal system. The longitudinal layer structure is shown (top) along with an exploded view of a single double-layer (bottom-right). The transverse view of the flower petal arrangement of modules as seen from the direction of the beam (bottom-left).

energy in the first twenty layers of the ECal ($E_{20}$) to be no more than 1.5 (3.16) GeV for the 4 (8) GeV beam. Multi-electron events can be removed from the sample by checking the Trigger Scintillator, Tagger Tracker, and Recoil Tracker subsystems for multiple tracks. These trigger thresholds were optimized for the missing momentum analysis search channel in both the 4 GeV [13] and 8 GeV [15] beam cases and found appropriate for this ECal as Target (EaT) missing energy search as well.

## 3 Simulated samples

Samples of events corresponding to several physical processes are simulated in order to design the missing energy analysis and estimate the sensitivity of this technique to DM production. The samples used for this study were generated with version 10.2.3 of the Geant4 detector simulation toolkit [16] with patches to nuclear interaction cross sections and kinematics that are important for LDMX's beam energies [10] utilizing LDCS [17] for large-scale sample production. The background and signal samples share the same beam assumptions, namely that electrons arrive upstream of the tagging tracker system with a kinetic energy of 4 or 8 GeV. Each event is simulated with exactly one incoming beam electron.

In order to avoid simulating events that would be removed with a tracker-based requirement for the electron to have a certain minimum momentum, events where the primary electron falls below 87.5% of the beam energy before arrival at the face of the ECal are rejected in all samples. Based on simulation studies, we expect 62% of electrons which enter LDMX at full energy to meet this requirement.

Dedicated samples are produced for the signal and unbiased background processes, which are further complemented by dedicated samples for showers that impart significant momentum into nuclei systems ("enriched nuclear") or produce muons ("di-muon"). More efficient production of simulation events is achieved by artificially increasing the cross section of chosen processes by some factor (the biasing factor) for particles above a certain energy threshold (the biasing threshold). For example, in the photo-nuclear background simulation, the photo-nuclear interaction cross section is increased for photons whose energy is above the biasing threshold. The event generation setup is also configured to simulate the interactions of all particles with total energy above the biasing threshold before any other particles in order to improve computational efficiency. Table 1 outlines the biasing and filtering for each of the samples used in this study and are explained in more detail in the following sections. Each of the samples was generated and analyzed separately. The unbiased background contains nuclear and di-muon background events, which are rare in the sample but can still be used to validate the biasing and filtering infrastructure. Since the nuclear and di-muon backgrounds are the dominant backgrounds for this analysis channel, the analysis methods are developed mainly using the biased samples for those background processes.

### 3.1 Signal

The signal samples were generated using the G4DarkBreM [18] technique in order to account for electron energy loss prior to undergoing a dark bremsstrahlung. The produced dark photon masses were 1, 5, 10, 50, 100, 500, and 1000 MeV. The production rate for masses above 100 MeV drops substantially necessitating an increased biasing factor as a function of mass (table 1) and leading to weaker sensitivities. When comparing these samples to other DM search literature, it is common to parameterize the DM phase space with an effective interaction strength $y$ and the mass of the candidate DM $m_\chi$ that would constitute the astronomical DM observed today. Here, these parameters relate to the DM model used within the simulation as

$$y = \alpha_D \epsilon^2 \left( \frac{m_\chi}{m_{A'}} \right)^4$$



JHEP12(2025)150

| Sample | Biasing Factor | Biasing Threshold |
|---|---|---|
| Signal | $m_{A'}^{\max(\log_{10}(m_A),2))}/\epsilon^2$ | $0.5E_{\text{Beam}}$ |
| Enriched Nuclear | 200 | $0.375E_{\text{Beam}}$ |
| Di-Muon | $10^5$ | $0.5E_{\text{Beam}}$ |
| **Sample** | **Filtering Cuts** | |
| Unbiased | $E_e \geq 0.875E_{\text{Beam}}$ | |
| Signal | $E_e \geq 0.875E_{\text{Beam}}$ & $E_{A'} \geq 0.5E_{\text{Beam}}$ | |
| Enriched Nuclear | $E_e \geq 0.875E_{\text{Beam}}$ & $E_{\text{nuc}} \geq 0.625E_{\text{Beam}}$ | |
| Di-Muon | $E_e \geq 0.875E_{\text{Beam}}$ & $E_\mu \geq 0.5E_{\text{Beam}}$ | |

**Table 1.** Configuration of the simulation samples used in this analysis. $E_{\text{beam}}$ is the beam energy being studied (4 or 8 GeV in this work). $m_A$ is the mass of the A' in MeV, $\epsilon$ is the dark photon mixing strength, $E_e$ is the energy of the primary electron at the front of the ECal, $E_{A'}$ is the energy of the generated A', $E_{\text{nuc}}$ is the total energy transferred to nuclear interactions during the event, and $E_\mu$ is the total energy of produced muons.

where $\alpha_D$ is the coupling between $A'$ and $\chi$ and we make standard, benchmark choices $\alpha_D = 0.5$ and $m_{A'} = 3m_\chi$ connecting the free parameters $(y, m_\chi)$ and $(\epsilon, m_{A'})$.

In addition to the selection on the primary electron's energy upon entering the ECal, events were also required to contain a dark photon with an energy of at least 50% of the beam energy produced in the ECal to avoid phase space outside of the trigger acceptance and improve computational efficiency.

Figure 3 shows the total energy deposited in the ECal as a fraction of the beam energy without trigger requirements for selected mass points for the 8 GeV beam case, with the 4 GeV beam case being very similar. The amount of energy deposited in the ECal for dark bremsstrahlung events is dependent on the mass of the dark photon. Dark photons with larger masses carry a larger amount of energy from the incident electron resulting in a shift of the total energy reconstructed in the ECal towards smaller values.

### 3.2 Enriched nuclear background

While the majority of interactions in the electron shower are electromagnetic, producing photons, electrons, and positrons, hadronic showers are occasionally produced from EN and PN interactions with nuclei in the ECal. The response of the ECal to these particles can be significantly smaller than for pure electromagnetic showers. Hadrons have significantly longer interaction distances in the dense materials of ECal compared to photons, electrons, and positrons, which can result in them escaping the calorimeter. For this reason, both EN and PN interactions are prominent backgrounds for this analysis. Since both electrons and photons exist within the developing shower, one cannot easily separate these interactions into distinct processes in the EaT search; therefore, both types of nuclear interactions are included in this "enriched nuclear" background.

For the simulation, both EN and PN interactions are biased by the same factor of 200 in order to maintain relative differences in rates. The energy threshold above which particles



JHEP12(2025)150

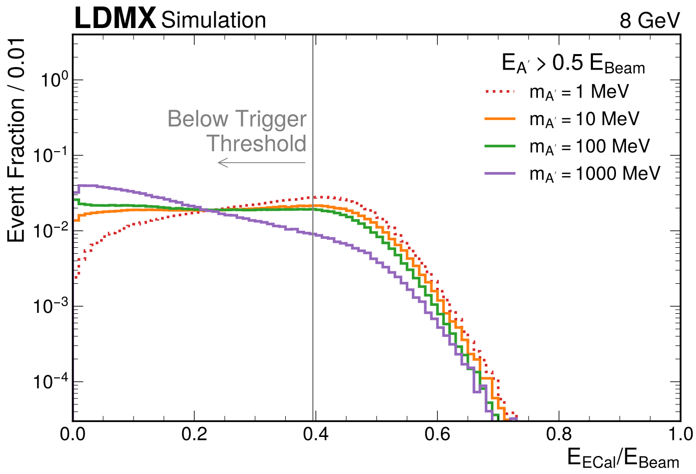


**Figure 3.** The total reconstructed energy summed over all layers in the ECal ($E_{\mathrm{ECal}}$) as a fraction of the beam energy ($E_{\mathrm{Beam}}$) for selected mass points, shown for the 8 GeV beam case. Heavier dark photons carry a larger amount of energy from the incident electron resulting in a shift of the total reconstructed energy in the ECal towards smaller values. The gray line indicates the trigger threshold. All distributions are normalized so their integral equals one.

are biased is set to 37.5% of the beam energy. A running total of the energy transferred from the initiating electron or photon to the nucleus (so-called "nuclear energy") is kept in each step of the simulation.

Only events where the total nuclear energy for all particles above the biasing threshold is greater than 62.5% of the beam energy are kept. The 62.5% energy threshold was chosen based on the features displayed in figure 4 which shows distributions of the total ECal energy based on the amount of nuclear energy in unbiased background events.

In order to avoid confining processes to a single nuclear interaction, the biasing and sorting threshold needs to be much less than the 62.5% total nuclear energy threshold. Moreover, the biasing and sorting threshold needs to be high enough to avoid simulating the entire shower before determining if an event should be kept. The value of 37.5% was found to be a good balance between these physical and computational bounds.

Figure 4 also highlights another background process for this analysis: photo-production of muon pairs. All of the simulated events in the low-nuclear-energy distribution below the trigger threshold are due to photon conversion to two muons.

### 3.3 Di-muon background

Simulating the di-muon background is simpler than the enriched nuclear background since it is a single process. The process is biased by a factor of $10^5$ ($10^4$) for 4 GeV (8 GeV) beam samples and only photons above half the beam energy are biased. The total energy of both muons produced ($E_\mu$) must be greater than half the beam energy in order for the event to be kept.

## 4 Analysis methodology

The signature of a dark bremsstrahlung event in the electromagnetic calorimeter is a single electromagnetic shower with significant energy loss relative to the beam energy. Figure 5

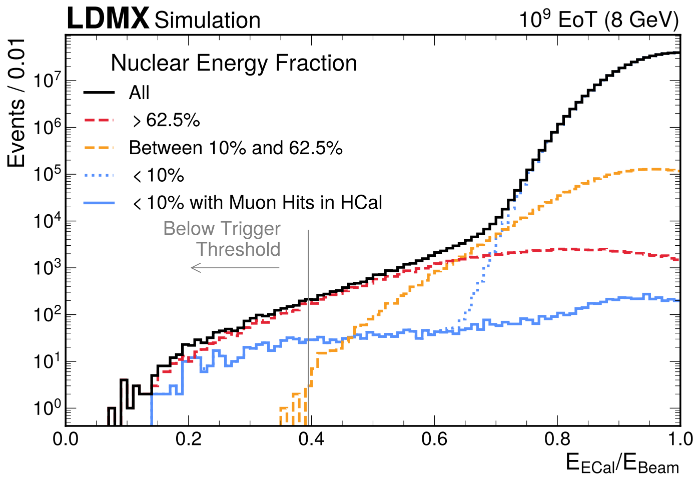


**Figure 4.** Total reconstructed energy in the ECal ($E_{\mathrm{ECal}}$) as a fraction of the beam energy ($E_{\mathrm{Beam}}$) depending on the total amount of simulated energy transferred to nuclear interactions (the "Nuclear Energy Fraction") for an unbiased sample of $10^9$ EoT. The maximum ECal energy allowed to pass the trigger is drawn in light gray. The elongated tail of the blue distribution (Nuclear Energy Fraction $< 10\%$) is due to photon conversion to muon pairs as evidenced by simulated energy deposits caused by muons within the HCal ("Muon Hits in HCal"). Events with $E_{\mathrm{ECal}} > E_{\mathrm{Beam}}$ due to resolution effects are omitted from this plot.

compares background to various signal mass points using the unit area normalized distributions of total reconstructed energy in the ECal summed over all layers. As the EaT search is designed to operate with early data samples when the trigger energy scale may not be fully calibrated, the energy requirement for event selection is tightened at the analysis level; the sum for the energy is performed over all 34 layers of the calorimeter and the threshold is set 400 MeV lower than what was required by the trigger. Therefore, for the 8 GeV beam the fully-calibrated sum over all layers $E_{\mathrm{ECal}}$ must be less than 2.76 GeV, while for the 4 GeV beam $E_{\mathrm{ECal}}$ must be less than 1.1 GeV. The sample with a full energy sum greater than the selection threshold but an $E_{20}$ below the trigger threshold will serve as a side band sample for evaluating the prediction for a range of backgrounds.

After the total energy requirement, the primary remaining backgrounds are those where a significant fraction of the energy is carried by neutrons, $K_L$, or muons through the ECal. To suppress these backgrounds, a requirement is placed on HCal that no scintillator bar in the detector is observed to contain a readout signal corresponding to more than 10 photo-electrons (PEs): $\max(\mathrm{PE}_{\mathrm{HCal}}) < 10$. For the side-HCal the measurement is made from a single photo-detector, while for the back-HCal the requirement is placed on the summed readout signal from the photo-detectors on both ends of the bar. The typical signal for a through-going muon in a single bar is 80 PE summed over both ends while the typical noise in a bar is 1 PE.

Some PN reactions produce several low-energy particles that range out in the ECal, often distributing a small amount of energy over a range of cells. To suppress such events, an additional upper limit on the overall width of the energy deposition in the ECal is applied. Each channel in the ECal which has an energy deposit above the readout threshold (corresponding to 50% of the energy deposited by a muon passing through a cell) is called a



JHEP12(2025)150

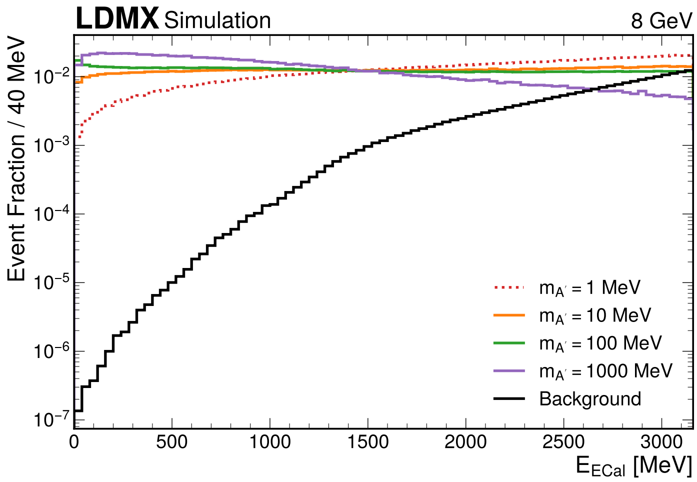


**Figure 5.** The total reconstructed energy summed over all layers of the ECal ($E_{\mathrm{ECal}}$) for all events that pass the trigger threshold. The signal and background distributions are normalized such that their integral is one. The events falling into bins with energy above the trigger threshold are omitted from this plot but included in efficiency calculations and the normalization.

"hit". The overall width of the energy deposition is then measured as the energy-weighted root-mean-squared spread (RMS) of the hit locations in the transverse plane, which quantifies the size of the event transverse to the particle impact direction on the calorimeter. This variable is typically larger for PN and EN backgrounds than for the single truncated electromagnetic shower present for a signal event. The event RMS is required to be less than 20 mm.

The variables used for selection are shown in figure 6. In this figure, the distributions are shown after all other selections are applied (including the trigger selection and the selection on the total ECal energy including all layers). The gray line indicates the selection on the observable in question, and the background sample is composed of the enriched nuclear and di-muon samples.

The final selection is tabulated in table 2. While not using the full power of the LDMX detector design, these simple cuts still reject enough background while keeping signal efficiencies high.

Figure 7 shows the signal and background total ECal energy distributions as a fraction of the beam energy after all selections are applied. With this selection of events, we can use the differing shapes between signal (close to uniform) and background (sharply falling) distributions in order to further improve the signal sensitivity. We fit the cumulative distribution of the background sample with a simple exponential function of the missing energy fraction and then use this fit to estimate the background yield within each of the three analysis bins. This fit utilizes the region above the final analysis threshold (dashed line in figure 7) and below the trigger threshold to help constrain it. Table 3 shows the results of this calculation. Moreover, this technique is well suited for first-contact with real data since the region currently constraining the fit would act as a control region enabling a data-driven background prediction. This fit is then used to give a background estimate and statistical uncertainty on this estimate in the three final analysis bins (edges shown in gray in figure 7).



JHEP12(2025)150

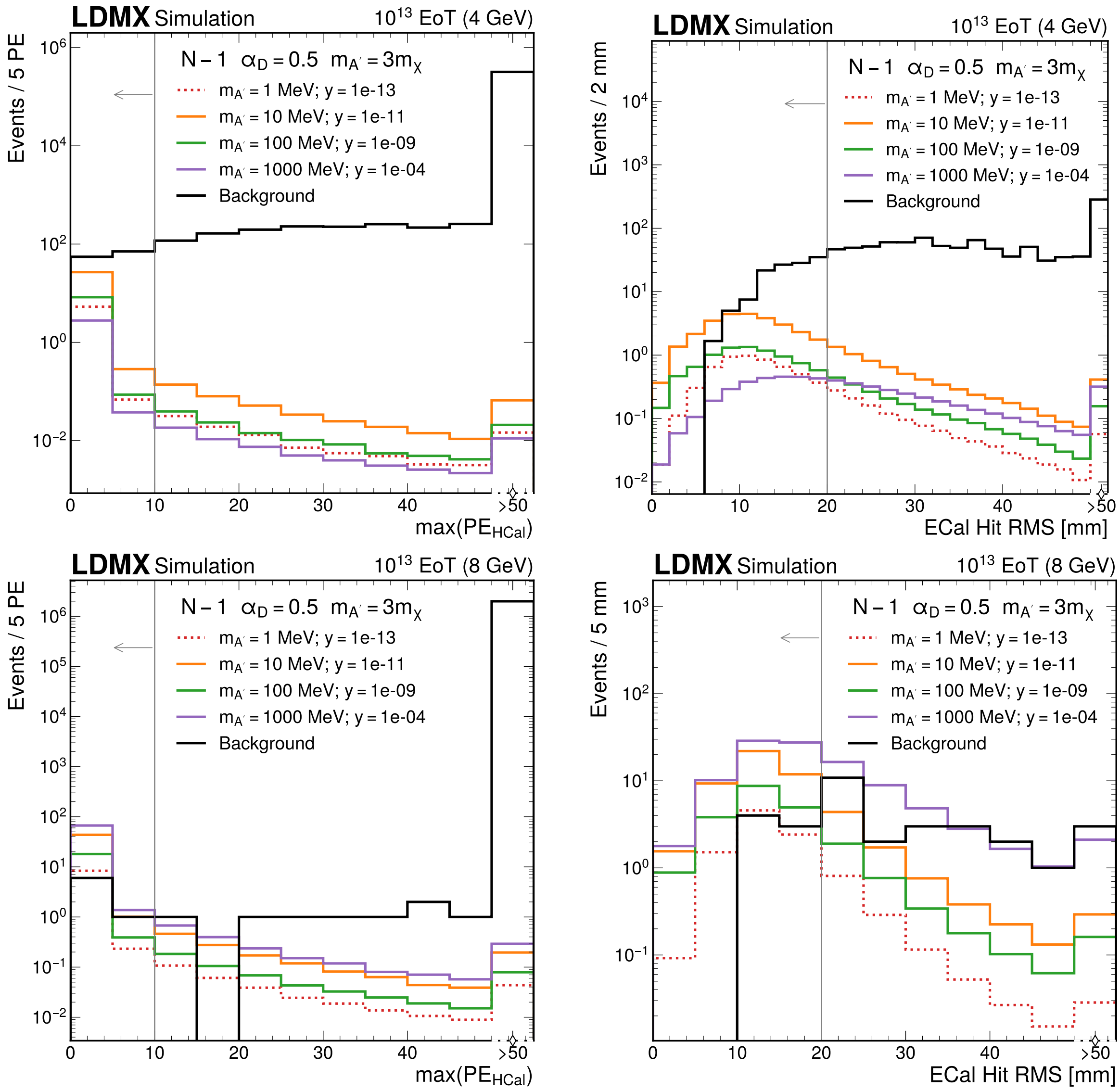


**Figure 6.** Variables used in signal selection for the EaT analysis channel. Each figure is an "N-1" plot where all other cuts are applied except for the variable in question. The signal samples are shown with a choice of effective interaction strength $y = \alpha_D \epsilon^2 (m_\chi / m_{A'})^4$ to which this analysis is sensitive. For empty bins, the uncertainty shown is derived from the Poisson uncertainty based on nearby bins. The gray line shows the selection cut. The background event counts correspond to the enriched nuclear and di-muon samples. The top (bottom) row shows the 4 GeV (8 GeV) beam.

Correlated systematic uncertainties on this background prediction were also estimated. Systematic uncertainties arising from 10% uncorrelated ECal mis-calibrations were estimated at 5% for all three final bins. Uncertainty in the background rate from 10 PE fluctuations of the maximum PE deposited in the HCal was also determined, resulting in no observable uncertainty in the lowest reconstructed ECal energy analysis bin and 60% (70%) in the middle (high) analysis bins. For the tracking requirements, while some misalignment may be expected for early analyses, this analysis does not see a strong dependence on the tracking requirement

JHEP12(2025)150

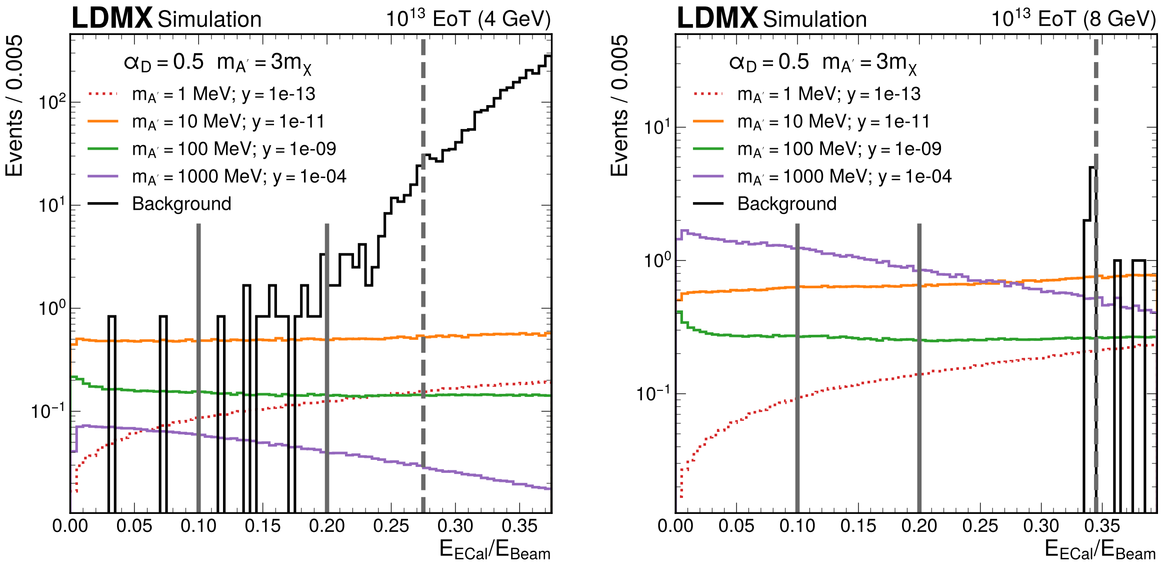


**Figure 7.** The total reconstructed energy in all layers of the ECal ($E_{\mathrm{ECal}}$) as a fraction of the beam energy ($E_{\mathrm{Beam}}$) for all samples that pass the selection criteria except the selection on ECal energy. The 4 GeV beam is shown on the left and the 8 GeV beam is shown on the right. The gray lines mark the edges of the analysis bins used to estimate the expected exclusion limit and the dashed line is the upper limit on the ECal energy which also serves as the upper limit of an analysis bin.

| Analysis Stage for 4 GeV Beam | Background Event Yield | Signal Efficiency (%) | | | |
|---|---|---|---|---|---|
| | | 1 MeV | 10 MeV | 100 MeV | 1 GeV |
| ECal Trigger ($E_{20} < 1.5$ GeV) | $5.11 \times 10^7$ | 58 | 67 | 71 | 83 |
| Tracker Requirement ($E_e > 3.5$ GeV) | $4.60 \times 10^7$ | 52 | 60 | 64 | 75 |
| ECal Energy ($E_{\mathrm{ECal}} < 1.1$ GeV) | $1.95 \times 10^6$ | 32 | 43 | 48 | 65 |
| $\max(\mathrm{PE}_{\mathrm{HCal}}) < 10$ | $1.15 \times 10^3$ | 31 | 42 | 47 | 62 |
| RMS Event Size $< 20$ mm | 126 | 25 | 33 | 37 | 30 |
| **Analysis Stage for 8 GeV Beam** | **Background Event Yield** | **Signal Efficiency (%)** | | | |
| | | 1 MeV | 10 MeV | 100 MeV | 1 GeV |
| ECal Trigger ($E_{20} < 3.16$ GeV) | $6.78 \times 10^7$ | 66 | 74 | 79 | 89 |
| Tracker Requirement ($E_e > 7$ GeV) | $6.10 \times 10^7$ | 59 | 67 | 71 | 80 |
| ECal Energy ($E_{\mathrm{ECal}} < 2.76$ GeV) | $6.88 \times 10^6$ | 47 | 57 | 62 | 76 |
| $\max(\mathrm{PE}_{\mathrm{HCal}}) < 10$ | 31.8 | 45 | 55 | 60 | 73 |
| RMS Event Size $< 20$ mm | 7 | 39 | 47 | 50 | 47 |

**Table 2.** Cut flow analysis comparing background and various signal hypotheses for the simple cuts used in this analysis. The event yield for the background sample is calculated using the event weights and represent the number of events out of $10^{13}$ EoT equivalent. The signal efficiency is relative to the simulation sample. The efficiency and event yield values on a given row are reported *after* the analysis stage of that row. The top table is the cut flow for the 4 GeV beam, and the bottom table is for the 8 GeV beam.

| Beam Energy | Bin 1 | Bin 2 | Bin 3 |
|---|---|---|---|
| 4 GeV | $0.87 \pm 0.09$ | $15.6 \pm 0.9$ | $127.6 \pm 3.4$ |
| 8 GeV | $0.08^{+0.25}_{-0.08}$ | $0.4^{+0.8}_{-0.4}$ | $4.7 \pm 1.2$ |

**Table 3.** Background prediction and its uncertainty on the number of events within the analysis bins.

and so it will be set such that 90% of tracks connected to full-energy clusters pass it. Based on simulation studies, the analysis will require a tracker performance reliable-enough to reject tracks below half the beam energy, which can be achieved with minimal alignment, so no systematic uncertainty is considered for the tracker.

## 5 Results

The expected reach of the EaT analysis in the $y - m_\chi$ plane is shown in figure 8 which used the COMBINE[19] statistical framework to perform a 3-bin expected exclusion estimate using the CLs criterion [20, 21] with the modified profiled likelihood ratio [22] as test statistic and using a log-normal model for nuisance parameters affecting yields. The signal yield limit estimated by COMBINE is converted to a limit on $y$ using an estimate of the expected production rate of dark photons from the simulation described above. This rate estimate is taken with a 20% systematic uncertainty representing uncertainty in the effective target material composition. The leading experimental systematic uncertainty is the HCal veto efficiency, which has a 10% impact on the expected sensitivity.

The EaT lines reflect the results from this study for the 8 GeV (orange) and 4 GeV (blue) beams. The red line is the LDMX Missing Momentum (MM) analysis sensitivity [13, 15] for a total exposure of $4 \times 10^{14}$ electrons-on-target. The EaT analysis is expected to achieve world-leading sensitivity in the early stages of LDMX operation, and to extend that sensitivity as the data sample increases. The MM search provides additional measurement possibilities to confirm an observation of DB such as the transverse-momentum distribution of the recoil electron, which can not be precisely measured in the EaT analysis channel.

## 6 Conclusions

The Light Dark Matter eXperiment will use a fixed-target, missing-momentum approach to perform a search across a range of mixing strengths for thermal-relic DM with a mass of 1 MeV to 1 GeV. This paper has described the use of the ECal as a secondary active target, which allows world-leading sensitivity in the early running stages of LDMX and provides a second analysis channel with different systematic uncertainties and background characteristics compared with the primary missing-momentum search channel. A detailed evaluation of this EaT analysis was described, employing a limited set of selection variables appropriate for use during early data-taking and evaluating the impact of a range of systematic uncertainties on the analysis result. These variables are sufficient to suppress the known background processes while maintaining substantial signal efficiency. The final background prediction and statistical analysis follows a structure that is applicable to beam data, preparing the



JHEP12(2025)150

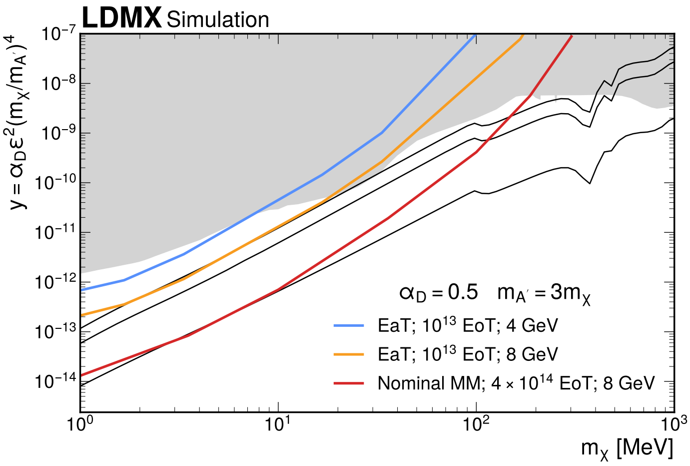


**Figure 8.** The 95% confidence level sensitivity of the EaT analysis for the 4 GeV (blue) and 8 GeV (orange) beam cases compared to other experiments led by NA64 [23], *BaBar* [24], and COHERENT [25] (gray); scalar, Majorana, and Pseudo-Dirac theory expectations (black, top-to-bottom); and the LDMX MM analysis sensitivity (red).

collaboration to conduct dark matter physics searches with a novel apparatus with only a few weeks of beam time.

As the beam sample size collected by LDMX grows, the EaT analysis channel is anticipated to maintain comparable exclusion sensitivity to the MM analysis by having access to a higher signal rate and through the staged introduction and validation of more advanced variables to suppress the backgrounds which will become relevant for larger detector exposures. The EaT analysis is therefore expected to complement the MM analysis and extend the reach of LDMX data.

## Acknowledgments


Support for UCSB is made possible by the Joe and Pat Yzurdiaga endowed chair in experimental science. Use was made of the UCSB computational facilities administered by the Center for Scientific Computing at the California NanoSystems Institute and Materials Research Laboratory (an NSF MRSEC; DMR-1720256) and purchased through NSF CNS-1725797, and from resources provided by the Swedish National Infrastructure for Computing at the Centre for Scientific and Technical Computing at Lund University (LUNARC), as well as LUNARC's own infrastructure. Contributions from Caltech, CMU, Stanford, TTU, UMN, UVA, and UCSB are supported by the US Department of Energy under grants DE-SC0011925, DE-SC0010118, DE-SC0022083, DE-SC0015592, DE-SC00012069, DE-SC0007838, and DE-SC0011702, respectively. Support for Lund University is made possible by the Knut and Alice Wallenberg foundation (project grant Light Dark Matter, Dnr. KAW 2019.0080), and by the Crafoord foundation (Dnr 20190875) and the Royal Physiographic Society of Lund. RP acknowledges support through the L'Oréal-UNESCO For Women in Science in Sweden Prize with support of the Young Academy of Sweden, and from the Swedish Research Council (Dnr 2019-03436). LB acknowledges support from the Knut and Alice Wallenberg





JHEP12(2025)150

Foundation Postdoctoral Scholarship Program at Stanford (Dnr. KAW 2018.0429). JE, GK, CH, WK, CMS, and NT are supported by the Fermi Research Alliance, LLC under Contract No. DE-AC02-07CH11359 with the U.S. Department of Energy, Office of Science, Office of High Energy Physics and the Fermilab LDRD program. CB, PB, OM, TN, PS, and NT are supported by Stanford University under Contract No. DE-AC02-76SF00515 with the U.S. Department of Energy, Office of Science, Office of High Energy Physics.

**Data Availability Statement.** This article has no associated data or the data will not be deposited.

**Code Availability Statement.** This article has no associated code or the code will not be deposited.



## References

[1] M. Battaglieri et al., *U.S. cosmic visions: new ideas in dark Matter 2017. Community report*, in the proceedings of the *U.S. cosmic visions: new ideas in dark matter*, (2017) [arXiv:1707.04591] [INSPIRE].

[2] J. Alexander et al., *Dark sectors 2016 workshop: community report*, arXiv:1608.08632 [INSPIRE].

[3] R. Kolb et al., *Basic research needs for dark-matter small projects new initiatives*, https://science.osti.gov/-/media/hep/pdf/Reports/Dark_Matter_New_Initiatives_rpt.pdf, (2018).

[4] G. Krnjaic et al., *A Snowmass whitepaper: dark matter production at intensity-frontier experiments*, arXiv:2207.00597 [INSPIRE].

[5] S. Gori et al., *Dark sector physics at high-intensity experiments*, arXiv:2209.04671 [INSPIRE].

[6] G. Lanfranchi, M. Pospelov and P. Schuster, *The search for feebly interacting particles*, *Ann. Rev. Nucl. Part. Sci.* **71** (2021) 279 [arXiv:2011.02157] [INSPIRE].

[7] P. Agrawal et al., *Feebly-interacting particles: FIPs 2020 workshop report*, *Eur. Phys. J. C* **81** (2021) 1015 [arXiv:2102.12143] [INSPIRE].

[8] R. Essig, J. Mardon and T. Volansky, *Direct detection of sub-GeV dark matter*, *Phys. Rev. D* **85** (2012) 076007 [arXiv:1108.5383] [INSPIRE].

[9] E. Izaguirre, G. Krnjaic, P. Schuster and N. Toro, *Analyzing the discovery potential for light dark matter*, *Phys. Rev. Lett.* **115** (2015) 251301 [arXiv:1505.00011] [INSPIRE].

[10] LDMX collaboration, *Light Dark Matter eXperiment (LDMX)*, arXiv:1808.05219 [INSPIRE].

[11] T. Åkesson et al., *Current status and future prospects for the Light Dark Matter eXperiment*, in the proceedings of the *Snowmass 2021*, (2022) [arXiv:2203.08192] [INSPIRE].

[12] LCLS-II collaboration, *LCLS-II: status of the CW X-ray FEL upgrade to the LCLS facility*, in the proceedings of the *37th international free electron laser conference*, (2015) [DOI:10.18429/JACoW-FEL2015-WEP014] [INSPIRE].

[13] LDMX collaboration, *A high efficiency photon veto for the Light Dark Matter eXperiment*, *JHEP* **04** (2020) 003 [arXiv:1912.05535] [INSPIRE].

[14] CMS collaboration, *The phase-2 upgrade of the CMS endcap calorimeter*, CERN-LHCC-2017-023, CERN, Geneva, Switzerland (2017) [DOI:10.17181/CERN.IV8M.1JY2].

[15] LDMX collaboration, *Photon-rejection power of the Light Dark Matter eXperiment in an 8 GeV beam*, *JHEP* **12** (2023) 092 [arXiv:2308.15173] [INSPIRE].

[16] GEANT4 collaboration, *GEANT4 — a simulation toolkit*, *Nucl. Instrum. Meth. A* **506** (2003) 250 [INSPIRE].

[17] L.K. Bryngemark et al., *Building a distributed computing system for LDMX — challenges of creating and operating a lightweight e-infrastructure for small-to-medium size accelerator experiments*, *EPJ Web Conf.* **251** (2021) 02038 [arXiv:2105.02977] [INSPIRE].

[18] T. Eichlersmith et al., *Simulation of dark bremsstrahlung in GEANT4*, *Comput. Phys. Commun.* **287** (2023) 108690 [arXiv:2211.03873] [INSPIRE].

[19] CMS collaboration, *The CMS statistical analysis and combination tool: combine*, *Comput. Softw. Big Sci.* **8** (2024) 19 [arXiv:2404.06614] [INSPIRE].

[20] T. Junk, *Confidence level computation for combining searches with small statistics*, *Nucl. Instrum. Meth. A* **434** (1999) 435 [hep-ex/9902006] [INSPIRE].

[21] A.L. Read, *Presentation of search results: the $CL_s$ technique*, *J. Phys. G* **28** (2002) 2693 [INSPIRE].

[22] G. Cowan, K. Cranmer, E. Gross and O. Vitells, *Asymptotic formulae for likelihood-based tests of new physics*, *Eur. Phys. J. C* **71** (2011) 1554 [*Erratum ibid.* **73** (2013) 2501] [arXiv:1007.1727] [INSPIRE].

[23] D. Banerjee et al., *Dark matter search in missing energy events with NA64*, *Phys. Rev. Lett.* **123** (2019) 121801 [arXiv:1906.00176] [INSPIRE].

[24] BaBar collaboration, *Search for invisible decays of a dark photon produced in $e^+e^-$ collisions at BaBar*, *Phys. Rev. Lett.* **119** (2017) 131804 [arXiv:1702.03327] [INSPIRE].

[25] COHERENT collaboration, *First probe of sub-GeV dark matter beyond the cosmological expectation with the COHERENT CsI detector at the SNS*, *Phys. Rev. Lett.* **130** (2023) 051803 [arXiv:2110.11453] [INSPIRE].


JHEP12(2025)150